Title: Structural evolution, grain growth kinetics and microwave dielectric properties of $Li_2Ti_{1-x}(Mg_{1/3}Nb_{2/3})xO_3$

Authors: J.J. Bian, X.H. Zhang

PII: S0955-2219(17)30577-0
DOI: http://dx.doi.org/10.1016/j.jeurceramsoc.2017.08.038
Reference: JECS 11433

To appear in: *Journal of the European Ceramic Society*

Received date: 25-4-2017
Revised date: 26-8-2017
Accepted date: 31-8-2017

Please cite this article as: Bian JJ, Zhang X.H.Structural evolution, grain growth kinetics and microwave dielectric properties of Li2Ti1-x(Mg1/3Nb2/3)xO3.*Journal of The European Ceramic Society* http://dx.doi.org/10.1016/j.jeurceramsoc.2017.08.038

Structural evolution, grain growth kinetics and microwave dielectric properties of $Li_2Ti_{1-x}(Mg_{1/3}Nb_{2/3})xO_3$

J.J. Bian* and X.H. Zhang

Department of Inorganic Materials, Shanghai University
333 Nanchen Road, shanghai 200444, China

*Corresponding author, Email address:jjbian@shu.edu.cn; Tel/Fax:86-21-66134799

$Li_2Ti_{1-x}(Mg_{1/3}Nb_{2/3})_xO_3$ ceramics were prepared by conventional solid state process. Their structural evolution, grain growth kinetics and microwave dielectric properties have been studied in this paper. The results show that continuous solid solution could be formed within the experiment compositional range. The structure changed from long range ordered monoclinic into short range ordered cubic phase as the increase in x. Small levels of substitution for $Ti^{4+}$by $(Mg_{1/3}Nb_{2/3})^{4+}$ slightly decreased the dielectric permittivity, while considerably improved the $Q\times f$ value. The temperature coefficient of resonant frequency changed from positive into negative value. The grain growth kinetics during sintering process and $Q\times f$ value of the sintered body were affected by different calcining temperature of mixed powders. Excellent combined microwave dielectric properties with ε_r ~21.0, $Q\times f$~200 000 GHz and τ_f value of ~ -1 ppm/℃ could be obtained after optimizing calcining temperature for the x=0.24 composition after sintering at 1250 ℃/2h.

Key Words: Lithium containing compound, Grain growth kinetics, Microwave dielectric properties

Introduction

Lithium containing rock salt compound with the composition Li_2TiO_3 was reported to have good microwave dielectric properties (ε_r~22.0, $Q\times f$~63,500 GHz and positive τ_f value of 20.3 ppm/℃) [1]. It undergoes an order-disordering phase transformation at the temperature range of 1150-1215℃[2-4]. The space group changes from monoclinic rock salt structure (C2/c) to cubic (Fm-3m) with the order-disordering phase transformation. Several types of lithium containing compounds with rock salt structure and their order-disordering phase transition behaviors have been reviewed in reference [5]. Based on the above investigations, various dopants have been tried to improve the dielectric properties of Li_2TiO_3. The microwave dielectric properties of Li_2TiO_3 could be remarkably improved by forming solid solutions with other rock salt type compounds such as MgO, Li_3NbO_4 and LiF[6-9]. The improvement of $Q\times f$ value can be ascribed to the disappearance of microcracks and possible stablization of the short range ordering domain boundaries in the ceramics. Recently, Guo hua Chen et al. investigated the microwave dielectric properties of $Li_2Ti_{1-x}(Zn_{1/3}Nb_{2/3})xO_3$ ($0<x<0.5$) solid solutions and found slight improvement of $Q\times f$ value compared with that of pure Li_2TiO_3 by complex substitution of $(Zn_{1/3}Nb_{2/3})$ for Ti^{4+} [10]. More recently, it was found that the dielectric properties could be considerably improved by forming $Li_2Ti_{1-x}(Al_{1/2}Nb_{1/2})_xO_3$ solid solutions[11]. The ordering degree and order-disordering transition temperature of Li_2TiO_3 usually decreases with the doping concentration [6-11]. The presence of short range ordering has been confirmed by Raman spectrum in many lithium containing

rock salt solid solution systems and also directly observed by HRTEM in MgO-doped Li_2TiO_3 [6,8,9,11,12]. Grain coalescence during sintering process and porous microstructure were also usually observed in Li_2TiO_3-based solid solution systems [6,8]. The grain growth kinetics and growth mechanism has not been clarified yet.

In the present work, the synthesizing condition, structural evolution and microwave dielectric properties of $Li_2Ti_{1-x}(Mg_{1/3}Nb_{2/3})xO_3$ ($0<x<0.6$) have been studied. In addition, the grain growth kinetics and the relationship between grain size, porosity and relative density have also been investigated in this paper.

Experimental

Samples of $Li_2Ti_{1-x}(Mg_{1/3}Nb_{2/3})xO_3$ ($0\leq x\leq 0.6$) were prepared using the conventional solid-state reaction method. Raw materials including Li_2CO_3 (99.9 %),TiO_2 (99.7 %), MgO (99.9 %),Nb_2O_5 (99.5 %) were weighed according to the stoichiometric ratio above and milled with ZrO_2 balls in alcohol for 24h.The slurries were dried and calcined at 800℃-1050℃ for 2h and milled for 24h again. The calcined powders were reground, granulated by mixing with 10% PVA as a binder. The granulates were then uni-axially pressed into cylinder pellet with 10mm in diameter and 4-5mm thick under the pressure of 10Mpa.The pellets were sintered at the temperature range from 1150 ℃ to 1300 ℃ for 2h. For the x=0.24 sample, the calcining temperature was optimized. In order to study its grain growth kinetics, three sets of sintering schedules were used, i.e. non-isothermal sintering, isothermal sintering and rapid heating. During the non-isothermal sintering experiments, the

samples were heated at constant heating rate of 5 ºC/min to the desired temperature (1150 ℃ to 1300 ℃) for 2h and then cooled to room temperature with furnace. Isothermal sintering was conducted at 1250 ℃. The samples were heated to a desired temperature at a heating rate of 5ºC/min and then held at this temperature for 0.5-3.5h. For fast firing, the samples were put into the furnace at 1250℃ and then held for 0.5-3.5h, after that the samples were took out and cooled at the room temperature.

The phase constituents of the sintered samples were identified by X-ray powder diffraction (XRD) with Ni-filtered CuKα radiation (40 kV and 20 mA, Model Dmax-RC, Japan). The Raman experiments were carried out for the sintered samples (RENIShaw in Via plus, UK). The Raman spectra were excited with the 514 nm line of a semiconductor laser at a power of 250 mW and recorded in back-scattering geometry using InVia Raman Microscope equipped with a grating filter, enabling good stray light rejection in the 100-1000 cm^{-1} range. Differential scanning calorimetry ((DSC), NETZSCH STA 449F3，Netzsch Instrumen，Germany) spectrums were measured to observe the order-disordering phase transition temperature. The microstructure of the sintered samples was observed by scanning electron microscopy ((SEM) Supra55, Carl Zeiss, Germany). All the samples were polished and thermally etched at the temperature of 50℃ lower than its sintering temperature for 30min. Grain sizes were measured from SEM micrographs of the etched samples by the Image-Pro Plus software. The lattice parameters and theoretical densities of the sample were refined via Jade 6.5 software. The densities of the ceramics were measured by the Archimedes method. Microwave dielectric properties of the sintered

specimens were measured at about 7–12 GHz using a network analyzer (modelN5230A, Agilent, Palo Alto, CA).The quality factor was measured by the transmission cavity method. The relative dielectric constant was measured according to Hakki–Coleman method with the TE_{011} resonant mode, and the temperature coefficient of the resonator frequency were measured using invar cavity at the temperature range from 20 ℃ to 80 ℃.

Result and Discussion

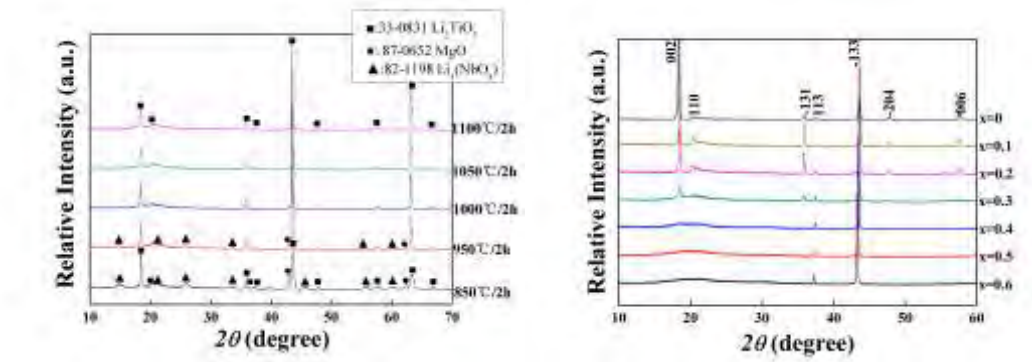

(a) (b)

Fig.1 Powder XRD patterns of (a) x=0.24 composition calcined at different temperatures and (b) $Li_2Ti_{1-x}(Mg_{1/3}Nb_{2/3})_xO_3$ ($0<x<0.6$) ceramics sintered at 1250℃ /2h.

Li_3NbO_4 and MgO secondary phases present in the sample calcined at the temperature ≤ 950 ℃/2h (Fig.1a). The amounts of secondary phases decrease with increasing calcining temperature and pure rock salt type phase could be obtained after calcining at the temperature≥1000 ℃/2h. All compositions exhibit a single rock salt type phase after sintering at 1250℃ for 2h regardless of the calcining temperature,

which means that continuous solid solutions were formed (Fig,1b). Note that the ordering degree indicated by the intensity of (002) reflection decreased with the increase in x and thus the structure changed from ordered monoclinic phase (C2/c) into disordered cubic phase (Fm3m) when x>0.3, which is similar to those previously reported for other Li_2TiO_3 based solid solutions[6-11]. The DSC spectra recorded at cooling stage for different composition (Fig.2) also indicates that the order-disordering phase transition temperature decreases with increasing substitution content, which is consistent with the result of XRD.

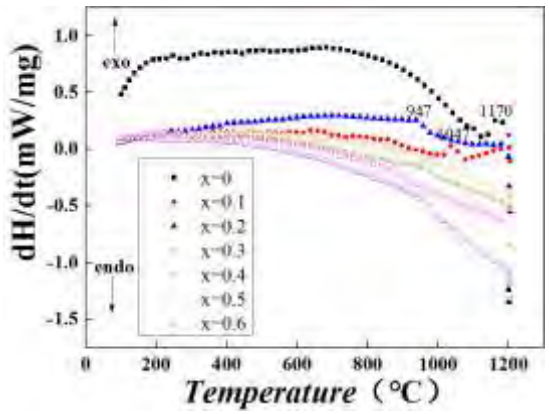

Fig.2 DSC spectra recorded at cooling stage for $Li_2Ti_{1-x}(Mg_{1/3}Nb_{2/3})_xO_3$ (0<x<0.6) .

Note that the x=0.3 composition seems to demonstrate disordering phase from its DSC curve without any corresponding thermal peak. However, small degree of ordering could still be observed from its XRD pattern shown in Fig.1b. It seems to imply that the phase transition is losing its first-order character and becoming more continuous in nature. The DSC peak for pure Li_2TiO_3 in this case shows that the order-disordering transition temperature is about 1170 ℃， which is slightly different from that reported previously[2-4]. We think the scattering data of the transition

temperature for Li_2TiO_3 may be related to the possible presence of defect associate with the lithium evaporation at high temperature. The Raman spectra recorded for the doped compositions ($x<0.3$) exhibit very similar Raman active bands to those of monoclinic Li_2TiO_3 reported previously [13,14] due to the forming of continuous solid solutions (Fig.3).

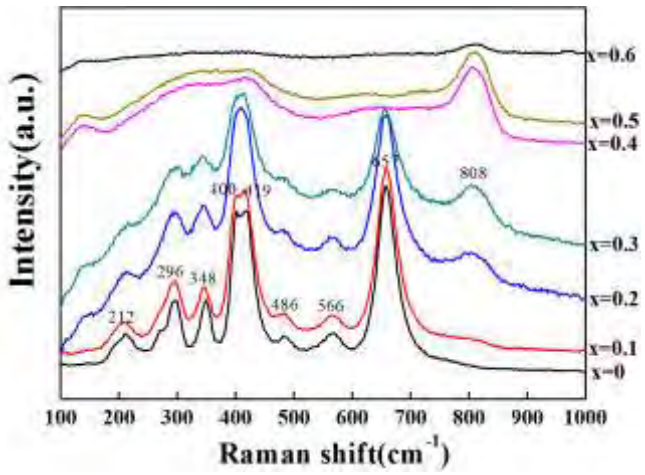

Fig.3 Raman spectra recorded for $Li_2Ti_{1-x}(Mg_{1/3}Nb_{2/3})_xO_3$ ($0<x<0.6$) ceramics sintered at 1250℃/2h.

The decrease in band intensity with increasing doping content indicates the decrease in cation ordering degree, which is also in well agreement with the XRD result. Furthermore, short range ordering could be confirmed as evident by the presence of weak broaden bands, which is supposed to be absent in the $x>0.3$ compositions with long range disordered face-centered cubic structure as shown in Fig.1b, according to group theory analysis. Note a new band at 808 cm^{-1} being consistent with the symmetric vibration of NbO6 octahedron appears when $x\geq0.2$. Similar phenomenon was also observed in the Li_2TiO_3-LiF and $Li_2Ti_{1-x}(Al_{1/2}Nb_{1/2})xO_3$

systems[9,11]. The appearance of the band at 808 cm^{-1} may be related to the presence of short rage ordering in the high level doped compositions.

Typical SEM images of the doped ceramics calcined at different temperatures after sintering at 1250℃for 2h exhibit single phase with porous microstructure (Fig.4). Grain coalescence and pore entrapment could be observed.

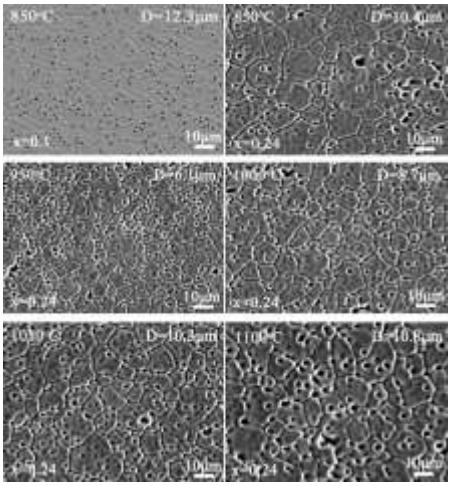

Fig.4 Typical secondary electron SEM images of the doped compositions calcined at different temperatures after sintering at 1250℃/2h.

The backscattering SEM image (ESI, S-Fig.1) and corresponding EDS analysis for x=0.2 composition sintered at 1250 ºC/2h demonstrates a little compositional fluctuation, which is within the uncertainty of the EDS technique. Pure Li_2TiO_3 exhibits the onset of the grains coalescence at the temperature of 1150 ºC (ESI, S-Fig.2), which is very close to its order-disordering phase transition temperature. Rapid grain growth occurred and eventually developed into a closed pore microstructure above 1200 ℃(ESI, S-Fig.2). For the general abnormal grain growth, the driving force for coalescence is boundary migration due to curvature, which

suggests that coalescence is favored at the large-small grain contacts. A large grain grows at the expense of fine grains. In contrast, contacting grains with similar size coalesced into a single grain in this case (inset ESI, S-Fig.2). It seems to imply that other causes including chemical gradients or strain state may be responsible for the grain coalescence in this case. The mobilities of ions, and hence the grain growth are expected to substantially increase when the phase changes from ordered into disordered state. The presence of defects due to lithium evaporation at high temperature (>1150 ºC), which is evident by the ~1.5 % weight loss after sintering and also consistent with calculation result by first principle[15]and thermogravimetric experimental result [16], would also facilitate the order-disordering phase transition and mass transportation, which in turn speed up the grain growth. The detail coalescence mechanism is being under further investigated by TEM analysis. For the doped compositions calcined at 850 ºC, average grain size is about 12 μm and changes little with composition, which is much smaller than that of pure Li_2TiO_3 (25μm) sintered at the same temperature. It suggests that the $(Mg_{1/3}Nb_{2/3})^{4+}$-codoping effectively suppressed the grain growth and improved densification compared with those of undoped one. The decrease in grain size for the doped compositions is believed to be caused by a solid-solution pinning mechanism[17]. Preferential faceting and micro-cracks caused by cleavage on (002), usually occurring in the pure Li_2TiO_3, disappeared in the doped compositions. It suggests that the doping suppressed both the grain growth and faceting due to the increase in disordering.

The average grain size decreases with increasing calcining temperature and minimum grain size of ~6μm could be reached for the sample calcined at 950℃/2h. Further increasing calcining temperature would lead to increase in grain size again. Note that the sample calcined at 950℃/2h demonstrates narrowest grain size distribution compared with those calcined at other temperatures (ESI-S-Fig.4). Grain growth depends on sintering temperature and time, which can be analyzed by well-known growth kinetics equation [18], i.e.

$$D^n - D_0^n = Kt \quad (1)$$

and

$$K = K_0 \exp\left(\frac{-Q}{RT}\right) \quad (2)$$

Where D is the average grain size at time t, D_0 is the average grain size at zero time, n is the growth exponent, K is a rate constant, K_0 is a pre-exponential constant, Q is the activation energy of grain growth, R and T has the common meaning. When D_0 is remarkably smaller than D, D_0^n can be neglected relative to D^n. Eq.(1) can be simplified as follows:

$$D^n = K_0 \exp\left(\frac{-Q}{RT}\right)t \quad (3)$$

When ln (D) is plotted versus ln (t), a straight line is obtained with the slope of 1/n (Fig.5a). Subsequently the activation energy, Q, can be obtained from the slope of an Arrhenious plot of $\ln(D^n/t)$ versus 1/T (Fig.5b). It is found that the x=0.24 composition calcined at different temperatures don't exhibit a parabolic grain growth with n larger than 2. This occurs because of the inconstant grain boundary mobility with grain size due to increase in solute drag and/or coalescences of pores and grains

as the grain size grow. The variation of n and corresponding activation energy for grain growth with calcining temperature is in well agreement with that for grain size. Compared with the pure Li_2TiO_3, $(Mg_{1/3}Nb_{2/3})^{4+}$ co-doping indeed increases the activation energy for grain growth, which can be used to explain why $(Mg_{1/3}Nb_{2/3})^{4+}$ co-doping leads to the suppression of grain growth. The doped sample calcined at 950 ℃/2h demonstrates largest value of n (3.5) and activation energy (Q=678 KJ/mol).

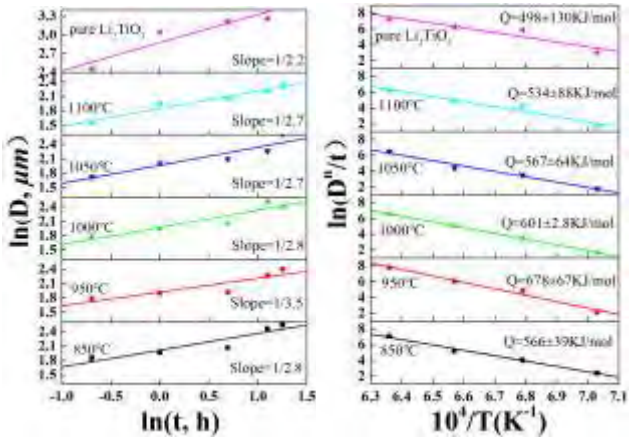

(a) (b)

Fig.5 (a) Plots of ln (D) versus ln (t) for x=0.24 composition calcined at different temperatures (b) Arrhenius plot of $\ln(D^n/t)$ versus 1/T for x=0.24 composition calcined at different temperatures.

Grain size –pore size trajectories (Fig.6) indicates that pore entrapment occurs above the temperature of 1200 ℃ regardless the calcining temperature. In contrast to the general later-stage sintering in which densification is accompanied by a decrease in pore size, pore coalescence during grain growth occurs above 1200 ℃ in this

case，which leads to the pores breaking away from the grain boundaries and leaving them isolated in the grains as shown in Fig.4. However, grain size–density trajectories (Fig.7) suggests that increasing the densification rate relative to the grain growth rate can be done for Li_2TiO_3 by $(Mg_{1/3}Nb_{2/3})^{4+}$ doping, optimizing calcining temperature and/or rapid firing cycle, as evident by flattening the grain size-density trajectory. The effect of calcining temperature on the densification and grain growth can be understood by considering the phase composition of the powder calcined at different temperature as shown in Fig.1a.

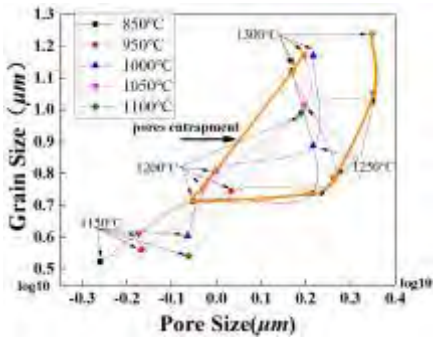

Fig.6 Grain size–pore size trajectories measured for x=0.24 composition calcined at different temperatures. The pore separation field is highlighted.

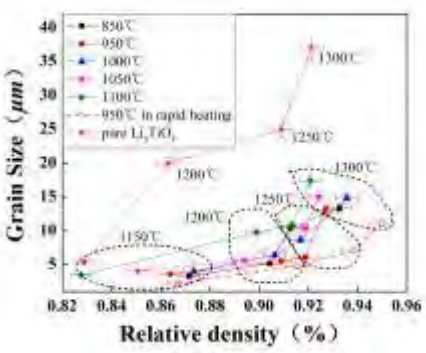

Fig.7 Grain size–density trajectories measured for x=0.24 composition calcined at different temperatures. For comparison, the data of pure Li_2TiO_3 are also provided.

Since isomorphic mixtures including Li_2TiO_3, MgO and Li_3NbO_4 presented in the powder calcined at the temperature ≤950 ℃/2h, sintering occurs simultaneously with homogenization via interdiffusion. Homogenization often dominating early stage of sintering occurs at ~1000 ℃ in this case. Chemical potential gradients caused by compositional gradients enhance the overall diffusional fluxes, and the interface between phases aids vacancy creation while retarding grain growth[19]. Large chemical potential gradients in the powder calcined at the temperature ≤850℃/2h enhance the grain growth. With the increasing calcining temperature, chemical potential gradients decrease due to increasing homogenization; hence the grain growth rate decreases. Although single phase solid solution formed with the further increase in calcining temperature (≥1000 ℃), the vacancy creation at the interface between phases retarding grain growth disappeared, which leads to the increase in grain size again.

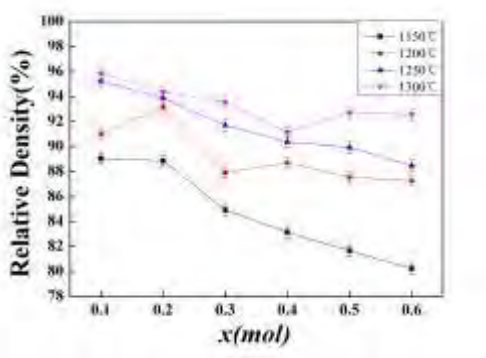

Fig.8 Variation of relative density of $Li_2Ti_{1-x}(Mg_{1/3}Nb_{2/3})_xO_3$ ($0<x<0.6$) calcined at 850℃after sintering at different temperatures.

The relative density increases compared with that of undoped and slightly decreases with further increasing doping, although it increases with increasing

sintering temperature for the fixed composition calcined at 850 ℃ (Fig.8). Corresponding microwave dielectric properties of the sintered samples are shown in Fig.9.

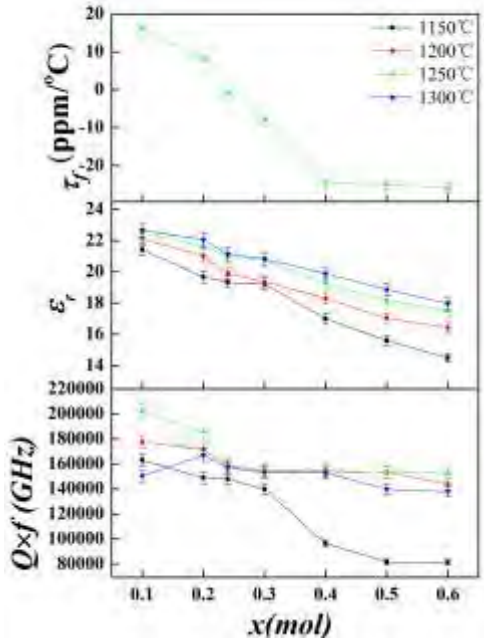

Fig.9 Microwave dielectric properties of $Li_2Ti_{1-x}(Mg_{1/3}Nb_{2/3})_xO_3$ ($0<x<0.6$) sintered at different temperatures.

The dielectric permittivity decreases with increasing x. The intrinsic factors reducing the dielectric permittivity could be ascribed to the decrease in layer charge imbalance with the decrease in ordering degree (ESI, S-Fig.3) and cationic polarizability. The decrease in relative density with increasing x (Fig.8) is another extrinsic factor reducing the dielectric permittivity. The optimized $Q\times f$ value is considerably improved by low levels of substitution with $(Mg_{1/3}Nb_{2/3})^{4+}$ for Ti^{4+} compared with that of pure Li_2TiO_3 regardless of high porosity left, while further

increase in substitution leads to the decrease in $Q\times f$ value. The substantial improvement of $Q\times f$ value may be related to the disappearance of micro-cracks, cleavages and possible stabilization of ordering domain antiphase-boundaries by low level substitution, which is similar to those previously reported for Li_2TiO_3-LiF and Li_2TiO_3-MgO systems [6,9]. The decrease in $Q\times f$ value with further increasing substitution can be ascribed to the decrease in ordering degree and relative density. Although both of the relative density and dielectric permittivity increase with the increase in sintering temperature until to 1300℃/2h for fixed composition, optimized $Q\times f$ value reaches at 1250℃/2h. Further increase in sintering temperature led to the reduction of $Q\times f$ value, which may be attributed to the increasing lithium evaporation during sintering process. The τ_f value decreases monotonically with increasing x. A near-zero τ_f value (-1.0 ppm/°C) could be obtained at x=0.24. The $Q\times f$ value of x=0.24 composition could be further improved from ~160000 to ~200000 GHz after optimizing calcining temperature at 950 ℃/2h (Fig.10) probably due to the homogenization of microstructure as discussed above.

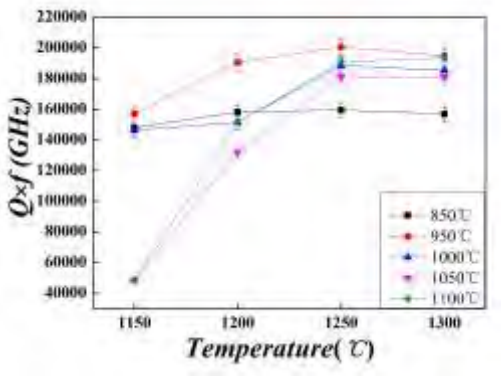

Fig.10 $Q\times f$ value for x=0.24 composition calcined at different temperatures after sintering at different temperatures for 2h.

Conclusions

Structural evolution, grain growth kinetics and microwave dielectric properties of $Li_2Ti_{1-x}(Mg_{1/3}Nb_{2/3})xO_3$ have been investigated in this paper. The crystal structure changed from layer ordered monoclinic into short-range-ordered cubic phase when x>0.3. The order-disordering transition temperature decreased with increasing x. Pore entrapment and porous microstructure could be observed in all compositions. Small level of $(Mg_{1/3}Nb_{2/3})^{4+}$-codoping (x=0.1) effectively suppressed the grain growth and improved densification compared with those of undoped one. The dielectric permittivity decreased with the increase in doping due to the decrease in layer charge imbalance. The $Q\times f$ value could be substantially improved by doping with $(Mg_{1/3}Nb_{2/3})^{4+}$(x=0.1) due to the improvement of microstructure including disappearance of microcracks and stabilization of ordering domain boundaries. The temperature coefficient of resonant frequency could be tuned from positive into negative value and near zero τ_f value reached at x= 0.24. Different calcining temperature of mixed powders would affect the grain growth kinetics during sintering process and $Q\times f$ value of the sintered body. The doped sample (x=0.24) calcined at 950℃/2h demonstrated largest activation energy (Q=678+67KJ/mol) for grain growth and narrowest grain size distribution. Rapid firing is also helpful to further increase the densification rate relative to the grain growth rate. Excellent combined microwave dielectric properties with $\varepsilon_r \sim 21.0$, $Q\times f$~200 000 GHz and τ_f value of ~ -1ppm/℃ could be obtained after optimizing calcining temperature at 950℃/2h for the x=0.24 composition after sintering at 1250℃/2h.

References

1. Yuan L.L. and Bian J.J. Microwave Dielectric properties of the lithium containing compounds with rock salt structure. Ferroelectrics 2009; 387: 1–7.

2. Izquierdo G., West A.R. Phase equilibria in the system Li_2O–TiO_2. Mater. Res. Bull. 1980;15:1655-1660.

3. Mikkelsen J.C. Pseudobinary phase relations of $Li_2Ti_3O_7$. J. Am. Cer. Soc. 1980;63 :331.

4. Kleykamp H. Phase equilibria in the Li-/Ti-O system and physical properties of Li_2TiO_3. Fusion Engineering and Design 2002; 61-62: 361-366.

5. Mather G.C, Dussarrat C., Etourneau J., West A.R. A review of cation-ordered rock salt superstructure oxides. J. Mater. Chem.2000;10:2219–30.

6. Bian J.J., Dong Y.F. New high Q microwave dielectric ceramics with rock salt structures:$(1-x)Li_2TiO_3$ + xMgO system ($0 \leqslant x \leqslant 0.5$). J. Eur. Ceram. Soc. 2010;30:325–330.

7. Huang C.L., Tseng Y.W., Chen J.Y., High-Q dielectrics using ZnO-modified Li_2TiO_3 ceramics for microwave applications. J. Eur. Ceram. Soc. 2012;32: 3287–3295.

8. Bian J.J., Wang L., Yuan L.L. Microwave dielectric properties of $Li_{2+x}Ti_{1-4x}Nb_{3x}O_3$ ($0 \leqslant x \leqslant 0.1$). Mater. Sci. Eng. B2009; 164: 96–100.

9. Ding Y.M. and Bian J.J. Structural evolution, sintering behavior and microwave dielectric properties of $(1-x)Li_2TiO_3$ + xLiF ceramics, Mater. Res. Bull., 2013; 48: 2776–2781

10. Chen G.H., Xu H.R., Yuan C.-L., Microstructure and microwave dielectric properties of $Li_2Ti_{1-x}(Zn_{1/3}Nb_{2/3})xO_3$ ceramics, Ceramics International 2013;39: 4887–4892.

11. Zhang T.W., Zuo R.Z. and Zhang J., Structure, microwave dielectric properties, and low-temperature sintering of acceptor/donor codoped $Li_2Ti_{1-x}(Al_{0.5}Nb_{0.5})xO_3$ Ceramics, J. Am. Ceram. Soc. 2016; 99 [3]L 825–832.

12. Leu L.-C., Bian J.J., Gout D., Letourneau S. and Ubic R., Order–disorder transition in the $(1-x)Li_2TiO_3$–xMgO system ($0 \le x \le 0.5$). RSC Advances 2012; 2: 1598 – 1604

13. Denisova T.A., Maksimova L.G., Polyakov E.V., Zhuravlev N.A., Kovyazina S.,Leonidova O.N.D., Khabibulin F., Yur'eva E.I., Metatitanic acid: Synthesis and properties Russ. J. Inorg. Chem. 2006; 51(5):691–699.

14. Bian J.J., Dong Y.F. Sintering behavior, microstructure and microwave dielectric properties of $Li_{2+x}TiO_3$ ($0 \leqslant x \leqslant 0.2$). Mater. Sci. Eng. B 2011;176: 147-151.

15. Murphy S.T. and Hine N. D. M. Point defects and on-stoichiometry in Li_2TiO_3, Chem. Mater. 2014;26:1629−1638.

16. Hoshino T., Dokiya M., Terai T., Takahashi Y., Yamawaki M. Non-stoichiometry and its effect on thermal properties of Li_2TiO_3. Fusion Engineering and Design 2002;61-62:353-60.

17. Chiang Y. M., Birnie D.P. and Kingery W. D. Physical ceramics-principles for ceramic science and engineering, John Wiley & Sons, Inc, New York1997.

18. Dutta S.K, and Sprigge R.M. Grain growth in fully dense ZnO. J. Am. Ceram. Soc. 1970;53(1):61-62.

19. German R.M., Sintering Theory and Practice, John Wiley & Sons, Inc, New York1996.

Caption list

Fig.1 Powder XRD patterns of (a) x=0.24 composition calcined at different temperatures and (b) $Li_2Ti_{1-x}(Mg_{1/3}Nb_{2/3})_xO_3$ ($0<x<0.6$) ceramics sintered at 1250℃/2h.

Fig.2 DSC spectra recorded at cooling stage for $Li_2Ti_{1-x}(Mg_{1/3}Nb_{2/3})_xO_3$ ($0<x<0.6$) .

Fig.3 Raman spectra recorded for $Li_2Ti_{1-x}(Mg_{1/3}Nb_{2/3})_xO_3$ ($0<x<0.6$) ceramics sintered at 1250℃ /2h.

Fig.4 Typical secondary electron SEM images of the doped compositions calcined at different temperatures after sintering at 1250℃/2h.

Fig.5 (a) Plots of ln (D) versus ln (t) for x=0.24 composition calcined at different temperatures (b) Arrhenius plot of $\ln(D^n/t)$ versus 1/T for x=0.24 composition calcined at different temperatures.

Fig.6 Grain size–pore size trajectories measured for x=0.24 composition calcined at different temperatures. The pore separation field is highlighted.

Fig.7 Grain size–density trajectories measured for x=0.24 composition calcined at different temperatures. For comparison, the data of pure Li_2TiO_3 are also provided.

Fig.8 Variation of relative density of $Li_2Ti_{1-x}(Mg_{1/3}Nb_{2/3})_xO_3$ ($0<x<0.6$) calcined at 850℃after sintering at different temperatures.

Fig.9 Microwave dielectric properties of $Li_2Ti_{1-x}(Mg_{1/3}Nb_{2/3})_xO_3$ ($0<x<0.6$) sintered at different temperatures.

Fig.10 $Q\times f$ value for x=0.24 composition calcined at different temperatures after sintering at different temperatures for 2h.

ESI

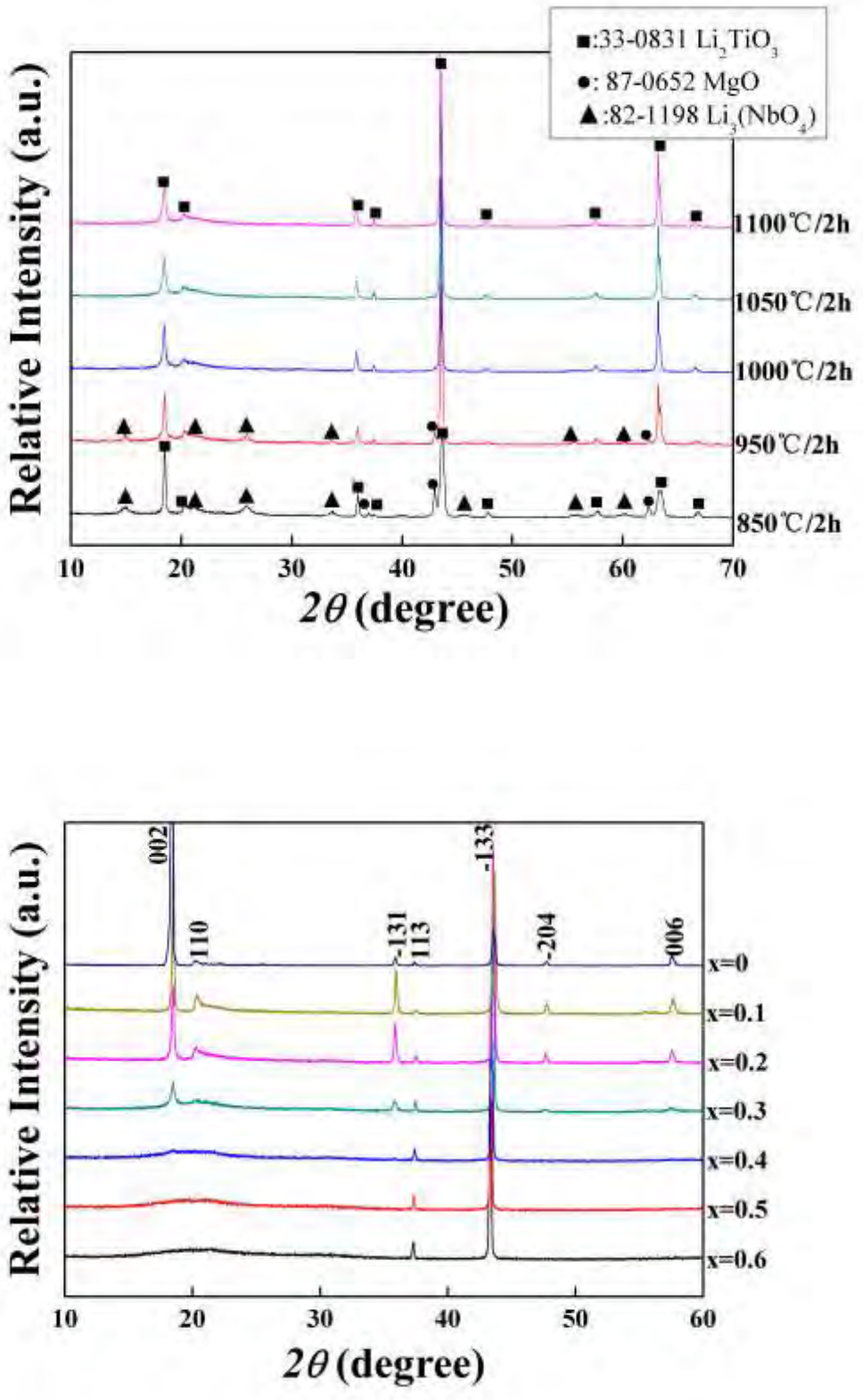

Fig.1

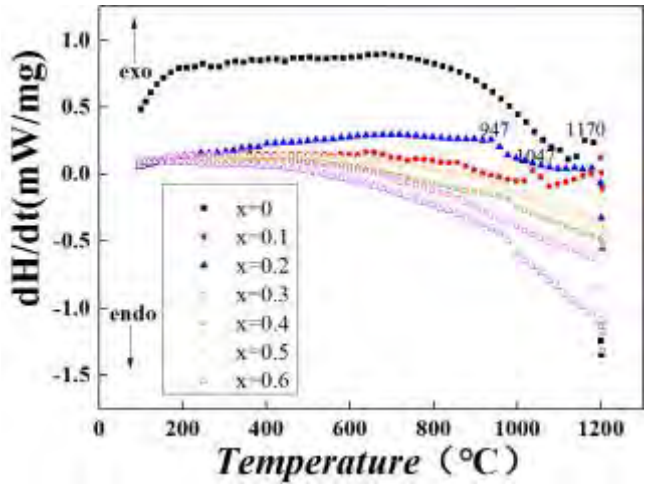

Fig 2

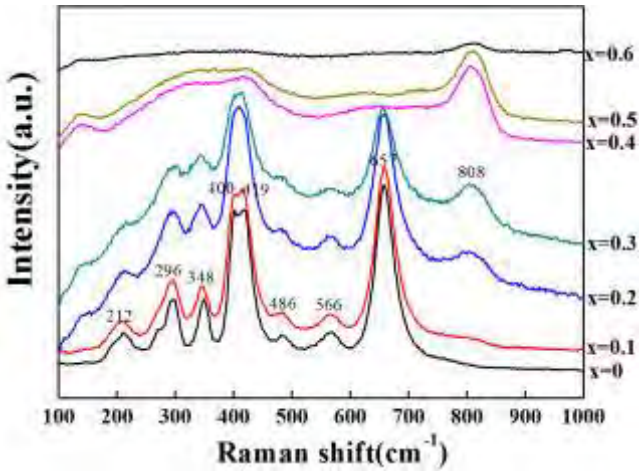

Fig 3

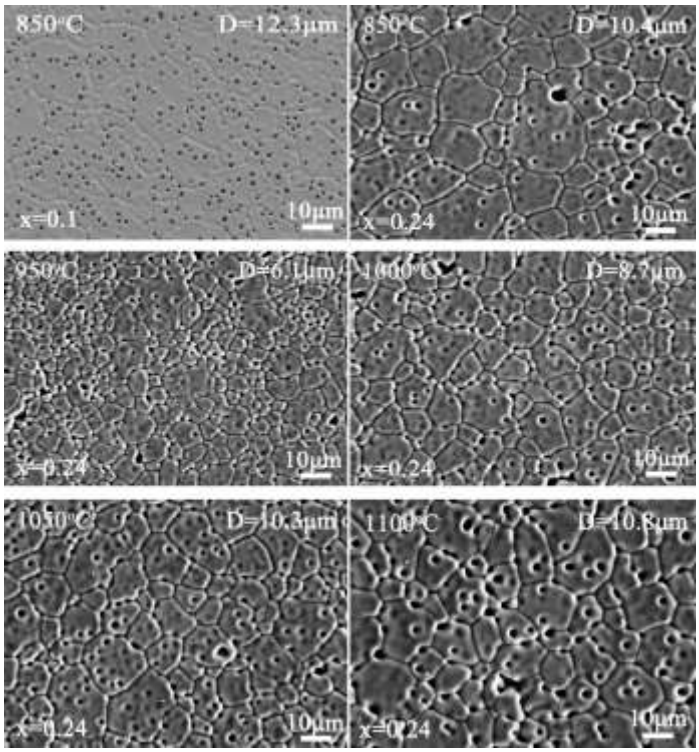

Fig 4

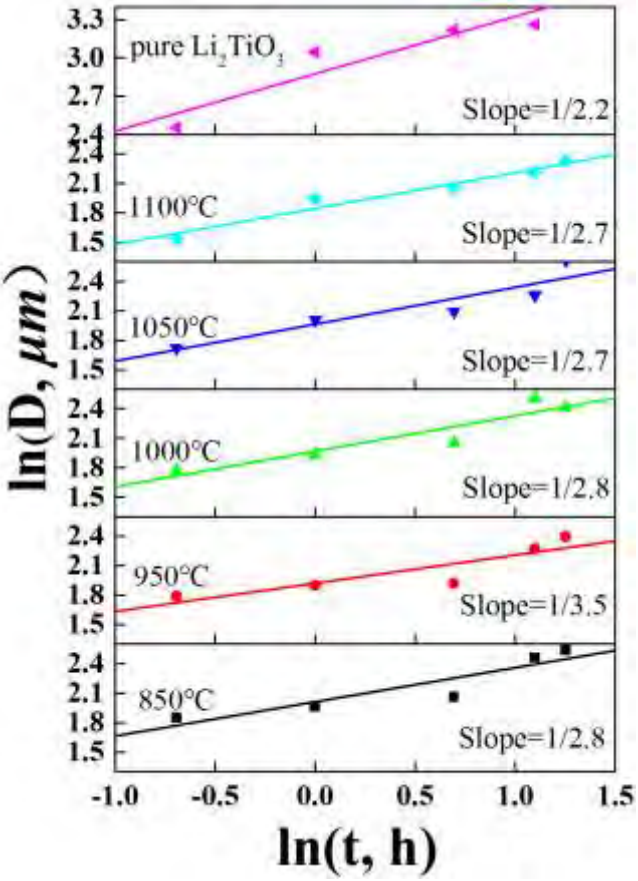

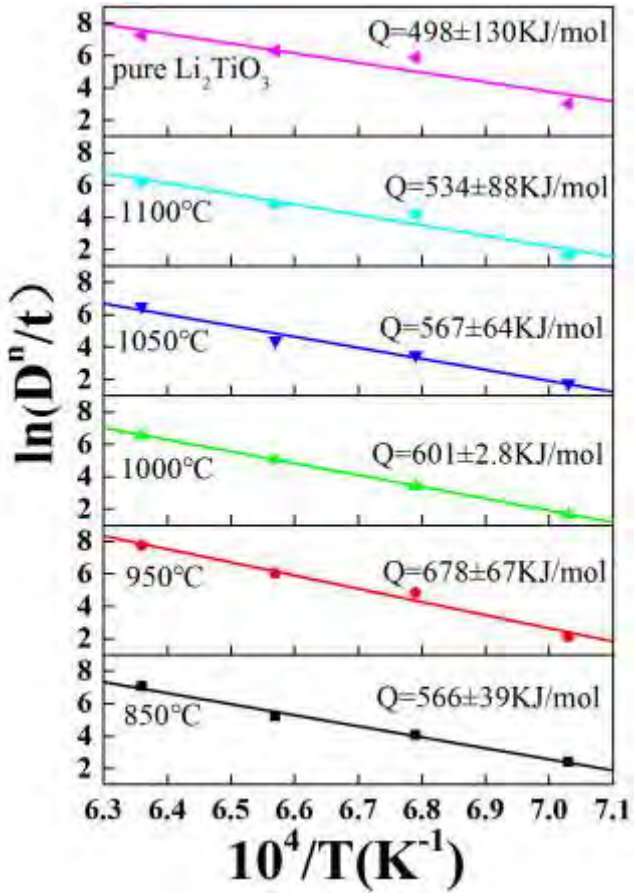

Fig 5

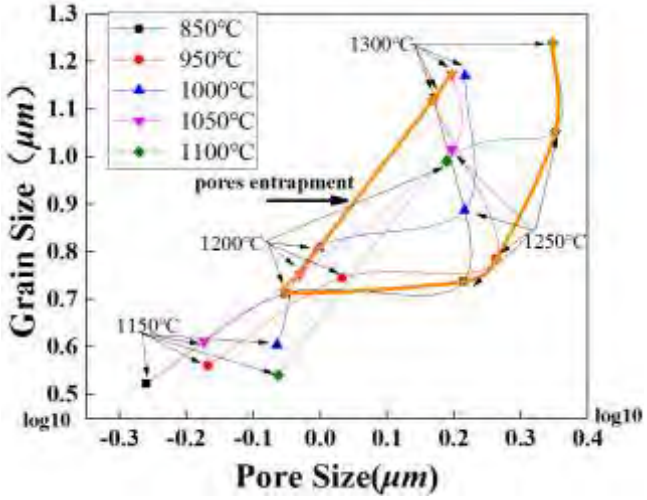

Fig 6

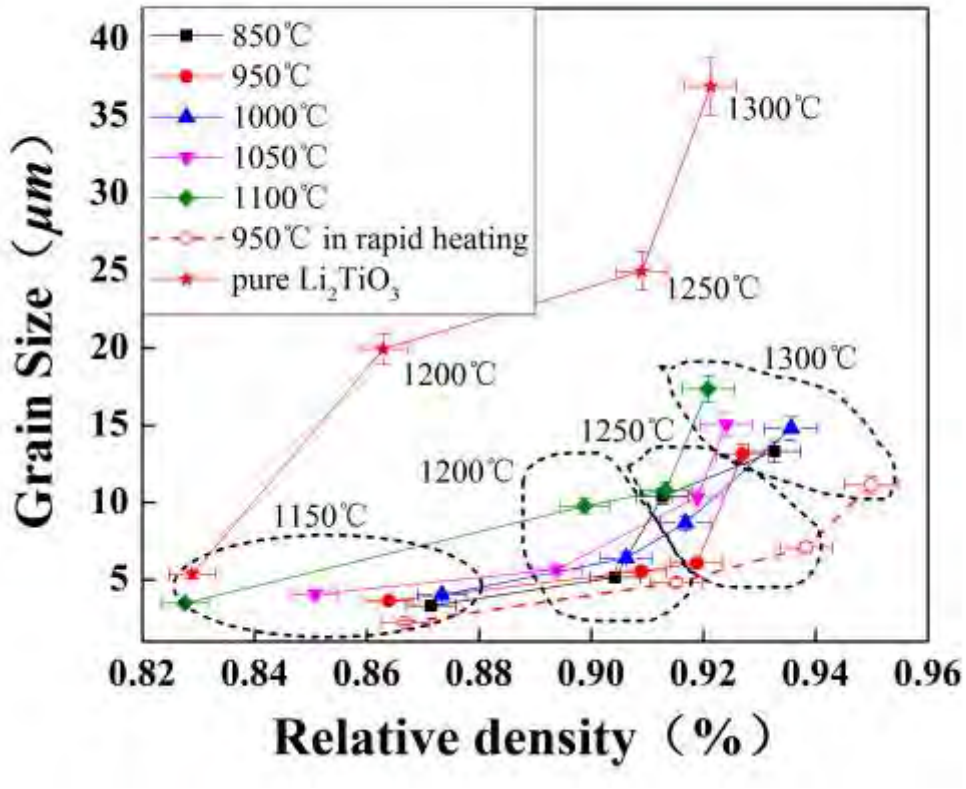

Fig 7

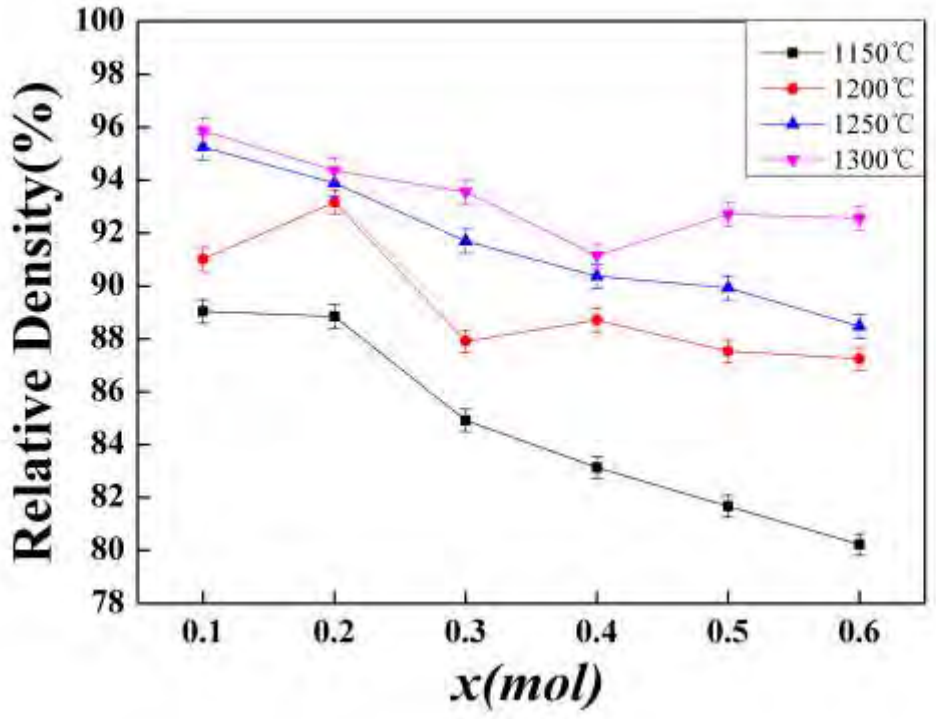

Fig 8

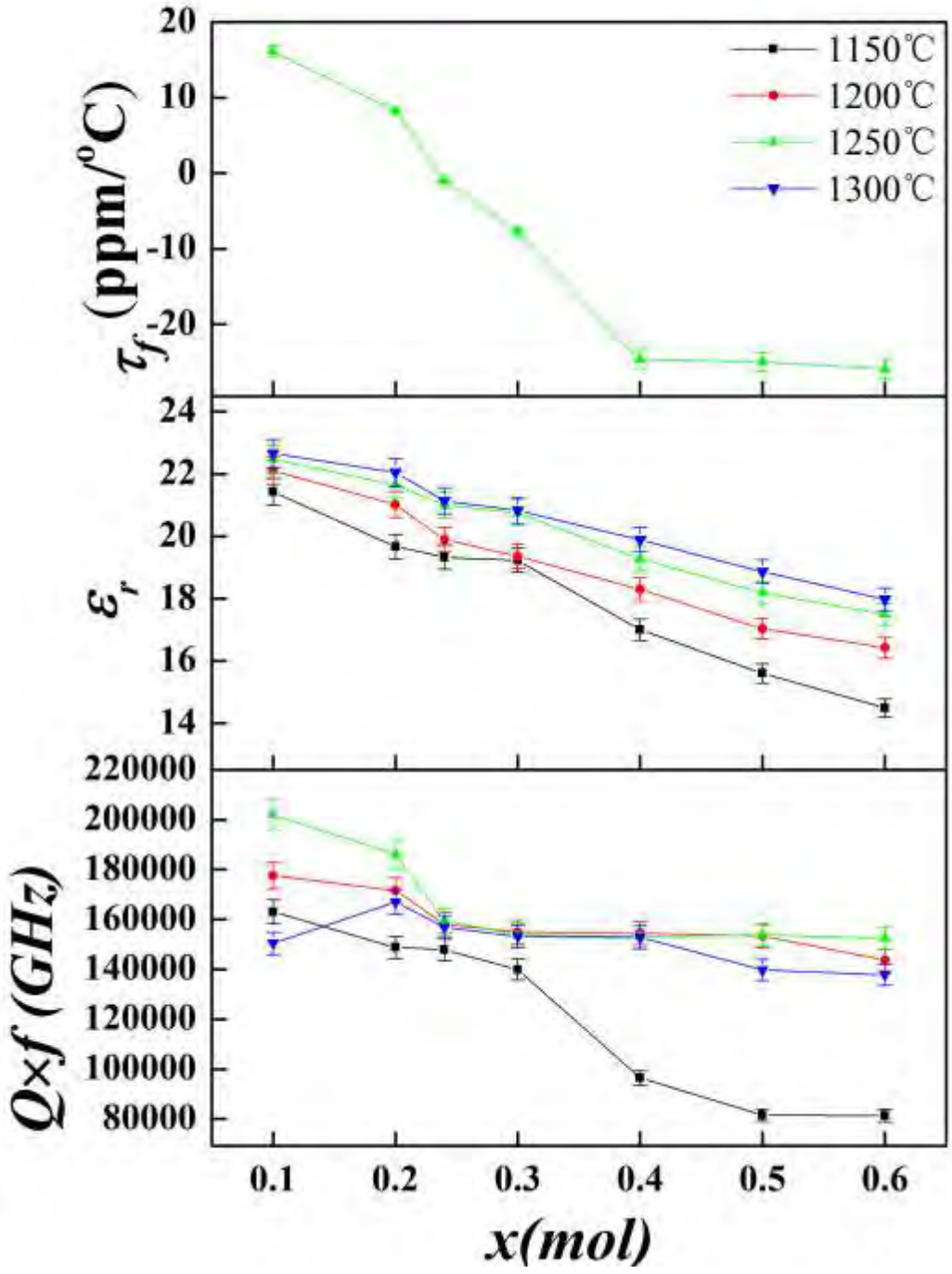

Fig 9

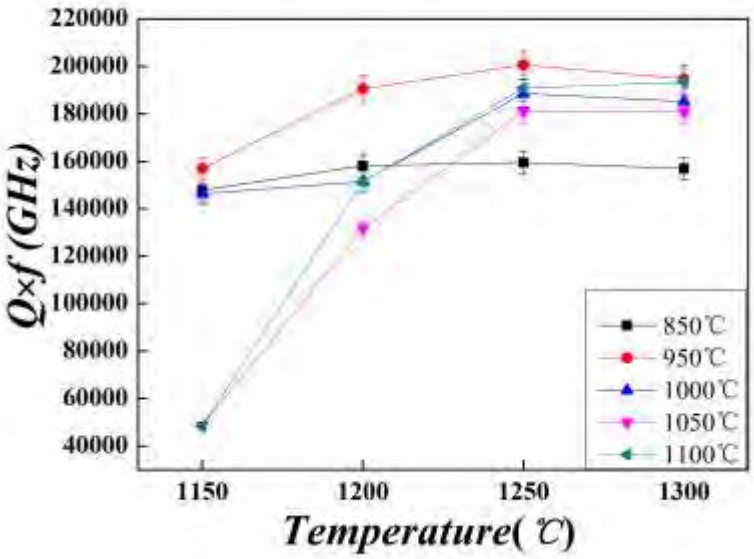

Fig 10